

Published in final edited form as:

Astrophys J Lett. 2016 October 10; 830(1): . doi:10.3847/2041-8205/830/1/L6.

The Spatial Distribution of Complex Organic Molecules in the L1544 Pre-stellar Core

Izaskun Jiménez-Serra^{1,2,3}, Anton I. Vasyunin^{4,5}, Paola Caselli⁴, Nuria Marcelino^{6,7}, Nicolas Billot⁸, Serena Viti², Leonardo Testi^{3,9}, Charlotte Vastel^{10,11}, Bertrand Lefloch^{12,13}, and Rafael Bachiller¹⁴

¹Astronomy Unit, School of Physics & Astronomy, Queen Mary University of London, Mile End Road, E1 4NS, London (UK)

²Department of Physics & Astronomy, University College London, 132 Hampstead Road, NW1 2PS London (UK)

³European Southern Observatory (ESO), Karl-Schwarzschild-Str. 2, 85748 Garching (Germany)

⁴Max-Planck-Institut für extraterrestrische Physik (MPE), Gießenbachstr., 85741 Garching (Germany)

⁵Ural Federal University, Ekaterinburg, Russia

⁶INAF, Osservatorio de Radioastronomia, Via P. Gobetti 101, 40129 Bologna, (Italy)

⁷Instituto de Ciencia de Materiales de Madrid, CSIC, C/ Sor Juana Inés de la Cruz 3, 28049 Cantoblanco (Spain)

⁸Instituto de Radioastronomía Milimétrica, Avenida Divina Pastora 7, E-18012 Granada (Spain)

⁹INAF-Osservatorio Astrofisico di Arcetri, Largo E. Fermi 5, I-50125 Firenze, Italy

¹⁰Université de Toulouse, UPS-OMP, IRAP, F-31400 Toulouse, France

¹¹CNRS, IRAP, 9 Av. Colonel Roche, BP 44346, F-31028 Toulouse Cedex 4, France

¹²Univ. Grenoble Alpes, IPAG, F-38000 Grenoble, France

¹³CNRS, IPAG, F-38000 Grenoble, France

¹⁴Observatorio Astronómico Nacional (OAN, IGN), Calle Alfonso XII 3, E-28014 Madrid, Spain

Abstract

The detection of complex organic molecules (COMs) toward cold sources such as pre-stellar cores (with $T < 10$ K), has challenged our understanding of the formation processes of COMs in the interstellar medium. Recent modelling on COM chemistry at low temperatures has provided new insight into these processes predicting that COM formation depends strongly on parameters such as visual extinction and the level of CO freeze out. We report deep observations of COMs toward two positions in the L1544 pre-stellar core: the dense, highly-extinguished continuum peak with

i.jimenez-serra@qmul.ac.uk.

This preprint was prepared with the AAS LATEX macros v5.2.

$A_V \sim 30$ mag within the inner 2700 au; and a low-density shell with average $A_V \sim 7.5$ -8 mag located at 4000 au from the core's center and bright in CH_3OH . Our observations show that CH_3O , CH_3OCH_3 and CH_3CHO are more abundant (by factors ~ 2 -10) toward the low-density shell than toward the continuum peak. Other COMs such as CH_3OCHO , $c\text{-C}_3\text{H}_2\text{O}$, HCCCHO , CH_2CHCN and HCCNC show slight enhancements (by factors ~ 3) but the associated uncertainties are large. This suggests that COMs are actively formed and already present in the low-density shells of pre-stellar cores. The modelling of the chemistry of O-bearing COMs in L1544 indicates that these species are enhanced in this shell because i) CO starts freezing out onto dust grains driving an active surface chemistry; ii) the visual extinction is sufficiently high to prevent the UV photo-dissociation of COMs by the external interstellar radiation field; and iii) the density is still moderate to prevent severe depletion of COMs onto grains.

Subject headings

astrochemistry — ISM; molecules — stars; formation — ISM; individual objects (L1544)

1 Introduction

Complex Organic Molecules (COMs) are carbon-based species with ≥ 6 atoms in their molecular structure (Herbst & van Dishoeck 2009). The most prolific regions in the detection of COMs in the interstellar medium (ISM) have been massive hot cores and Giant Molecular Clouds in the Galactic Center (SgrB2 (N) and (M); Hollis et al. 2000, 2006; Requena-Torres et al. 2008; Belloche et al. 2008, 2014) and low-mass hot corinos (IRAS16293-2422; Ceccarelli et al. 2000; Bottinelli et al. 2004; Jørgensen et al. 2012). Until recently, it was believed that COMs form on dust grains via hydrogenation (Charnley et al. 1995) or radical-radical reactions favoured by the heating from the central protostar (at $T \sim 30$ K; see Garrod et al. 2008). However, the detection of COMs such as propylene (CH_2CHCH_3), acetaldehyde (CH_3CHO), dimethyl ether (CH_3OCH_3) or methyl formate (CH_3OCHO) in dark cloud cores and pre-stellar cores with $T \sim 10$ K (B1-b, TMC-1, L1689B or L1544) has recently challenged our understanding of COM formation (Marcelino et al. 2007; Öberg et al. 2010; Bacmann et al. 2012; Cernicharo et al. 2012; Vastel et al. 2014; Loison et al. 2016).

Several mechanisms have been proposed to explain the presence of COMs in cold cores: gas-phase formation, non-canonical chemical explosions, cosmic-ray induced radical diffusion, impulsive spot heating of grains, or radical-radical recombination after H-atom addition/abstraction reactions on grain surfaces (Vasyunin & Herbst 2013; Rawlings et al. 2013; Balucani et al. 2015; Reboussin et al. 2014; Ivlev et al. 2015; Chuang et al. 2016). However, information about the spatial distribution of COMs in cold cores is lacking (as well as of their radial abundance profile probing different density and extinction regimes), which prevents us from testing these COM formation scenarios.

The detection of a low-density, CH_3OH -rich shell around the continuum peak of the L1544 pre-stellar core (Bizzocchi et al. 2014) offers a unique opportunity to test COM formation scenarios in cold sources. Species such as C_3O , ketene (H_2CCO), formic acid (HCOOH) and

acetaldehyde may be spatially co-located to CH₃OH in L1544 and may form at this low-density shell (Vastel et al. 2014). We report high-sensitivity observations of COMs toward two positions in the L1544 pre-stellar core: the continuum peak and a position within the low-density, CH₃OH-rich shell reported by Bizzocchi et al. (2014, hereafter the *CH₃OH peak*). Our results suggest that COMs are actively formed in the low-density shells of prestellar cores¹.

2 Observations

High-sensitivity single-pointing 3 mm observations were carried out toward two positions in the L1544 core during 10-16 December 2014 and 15-16 June 2016 with the Instituto de Radioastronomía Milimétrica (IRAM) 30 m telescope. We pointed our observations toward the core's dust continuum peak, $\alpha(\text{J2000})=5^{\text{h}}04^{\text{m}}17.21^{\text{s}}$, $\delta(\text{J2000})=25^{\circ}10'42.8''$, and toward the *CH₃OH peak*, $\alpha(\text{J2000})=5^{\text{h}}04^{\text{m}}18^{\text{s}}$ and $\delta(\text{J2000})=25^{\circ}11'10''$ (Bizzocchi et al. 2014). This position is $\sim 30''$ away from the core's center (~ 0.02 pc or 4000 au at 140 pc; Elias 1978).

The observations were done in wobbler-switched mode with an angular throw of $\pm 120''$. The dual sideband (2SB) EMIR E090 receivers were tuned at 84.37 GHz and 94.82 GHz with rejections ~ 10 dB. We used three slightly different central frequencies (84.36, 84.37, 84.38 GHz and 94.80, 94.82, 94.84 GHz) to avoid the appearance of weak spurious features in the spectra. The FTS spectrometer allowed us to observe the inner part of each 4 GHz sub-bands covering 7.2 GHz in total, and it provided a spectral resolution of 50 kHz (0.15 - 0.18 km s⁻¹ at 3 mm). The observed frequency ranges were 83.4-85.2, 86.7-88.5, 99.1-100.9, 102.4-104.2 GHz and 78.2-80.0, 81.4-83.2, 93.9-95.7, 97.1-98.9 GHz. Typical system temperatures were 70-120 K. The beam size was ~ 28 - $31''$ between 79-87 GHz, and ~ 24 - $26''$ between 94-103 GHz. Intensities were calibrated in units of antenna temperature, T_{A}^* , and converted into main beam temperature, T_{mb} , by using beam efficiencies of 0.81 at 79-100 GHz, and 0.78 at 103 GHz. The RMS noise level was 1.6-2.8 mK for the core's center position, and 2.2-3.7 mK for the *CH₃OH peak*.

3 Results

Figures 1 and 2 show some of the COM transitions detected toward L1544, while Table 1 lists all observed transitions and their derived line parameters. For completeness, we also provide the information about the covered transitions of acetaldehyde (CH₃CHO) – species already reported by Vastel et al. (2014) – and the upper limits of formamide (NH₂CHO), methyl isocyanate (CH₃NCO) and glycine (NH₂CH₂COOH). For all COMs the spectroscopic data were extracted from the JPL catalog (Pickett et al. 1998), except for dimethyl ether (CH₃OCH₃) for which we used SLAIM2, and cyclopropanone (c-C₃H₂O), methyl isocyanate and glycine, for which we used the CDMS catalog (Müller et al. 2005).

¹Part of these observations belong to the ASAI (Astrochemical Surveys at IRAM) program.

²The Spectral Line Atlas of Interstellar Molecules is available at <http://www.splatalogue.net> (Remijan et al. 2007).

Our high-sensitivity spectra reveal the detection of large COMs such as methyl formate (CH_3OCHO) and dimethyl ether (CH_3OCH_3) that had remained elusive in previous campaigns (see upper limits in Vastel et al. 2014). Other species detected are propynal (HCCCHO), cyclopropenone ($c\text{-C}_3\text{H}_2\text{O}$), ethynyl isocyanide (HCCNC) and vinyl cyanide (CH_2CHCN ; Figures 1 and 2). Methoxy (CH_3O), considered as a COM precursor or COM dissociation product, is also detected toward the $\text{CH}_3\text{OH peak}$. All these molecules are observed at the $\sim 10\text{-}20$ mK intensity level (Table 1). In Figure 1, we also report the tentative detection of methyl isocyanide (CH_3NC) toward the continuum peak. Its $\text{K}=0,1$ lines are detected at the 2.5σ and 3.2σ level. We are confident about the correct identification of all transitions since their derived radial velocities match the v_{LSR} of the source (7.2 km s^{-1}), and for most species at least two transitions are detected. In addition, we have looked for other lines that could be blended and have found none. Since the COM line profiles are narrow (linewidths $\sim 0.3\text{-}0.4 \text{ km s}^{-1}$; Table 1), it is unlikely that they appear blended with unknown species.

Table 1 shows that the line emission from O-bearing species is either brighter toward the $\text{CH}_3\text{OH peak}$ (by factors of $\sim 2\text{-}3$ for CH_3O , CH_3CHO , CH_3OCHO and CH_3OCH_3), or remains constant toward both positions (HCCCHO and $c\text{-C}_3\text{H}_2\text{O}$). The N-bearing COMs HCCNC , CH_3NC and CH_2CHCN , on the contrary, show an opposite behaviour with brighter emission seen toward the center of the core. As shown in Section 5, this behaviour translates into larger enhancements toward the $\text{CH}_3\text{OH peak}$ for CH_3O , CH_3CHO and CH_3OCH_3 than for the rest of COM species. Formamide, methyl isocyanate and glycine are not detected toward any position in L1544 (Table 1).

4 Excitation analysis of COMs

For CH_3O , CH_3OCHO , CH_3OCH_3 , CH_3CHO , CH_3NC and CH_2CHCN , we have detected several lines so that a multi-line excitation analysis can be performed. The excitation temperature, T_{ex} , and total column density, N_{obs} , of these molecules have been calculated using the MADCUBAIJ software (Martín et al. 2011; Rivilla et al. 2016), assuming extended emission and LTE conditions. Except for CH_3NC (which is tentatively detected; Section 3), the derived T_{ex} is $\sim 5\text{-}6$ K toward the core's center and $\sim 5\text{-}8$ K toward the $\text{CH}_3\text{OH peak}$ (Table 2). Errors in Table 2 correspond to 1σ uncertainties. We note that in some cases we had to fix T_{ex} to make MADCUBAIJ converge and find a solution. Since $c\text{-C}_3\text{H}_2\text{O}$ is not included in MADCUBAIJ, we used the Weeds software for this molecule (Maret et al. 2011) and assumed that its emission fills the beam.

For the COMs with only one transition detected (and also for the non-detections), we again used MADCUBAIJ and assumed extended emission and a T_{ex} range of $5\text{-}10$ K for both positions. This T_{ex} range agrees well with the values of T_{ex} obtained from the COM multiline excitation analysis (Table 2), and with the T_{ex} measured from CH_3OH by Bizzocchi et al. (2014). The estimated values of N_{obs} are reported in Table 2.

5 COM abundance profiles in L1544

By calculating the COM molecular abundances toward the two positions in L1544, we can provide constraints to the COM abundance profiles as a function of radius within the core. For the continuum peak, we need to calculate the H_2 column density, $N(H_2)$, within a radius of $13''$ or 1900 au (i.e. half the IRAM 30 m beam of our observations). The $N(H_2)$ of the core for radii ≤ 2500 au ($\sim 18''$ at 140 pc) is nearly flat with a radius dependence $N(H_2) \propto r^{-0.8}$ (Ward-Thompson et al. 1999). By using the peak $N(H_2)$ obtained by Crapsi et al. (2005, $9.4 \times 10^{22} \text{ cm}^{-2}$) for a radius of $6.5''$ (~ 910 au), we derive that $N(H_2) = 5.4 \times 10^{22} \text{ cm}^{-2}$ for a radius of $13''$ (1900 au). This value is similar to that estimated by Bacmann et al. (2000) for the same radius ($4.5 \times 10^{22} \text{ cm}^{-2}$; see their Table 2). The slight difference is due to the dust temperatures assumed in both calculations (12.5 K in Bacmann et al. 2000 vs. 10 K in Crapsi et al. 2005). Hereafter, we use $N(H_2) = 5.4 \times 10^{22} \text{ cm}^{-2}$ for the position of the continuum peak within a radius of $13''$.

For the CH_3OH peak, we assume an H_2 column density of $1.5 \times 10^{22} \text{ cm}^{-2}$ as derived by Spezzano et al. (2016) from Herschel data. The latter $N(H_2)$ corresponds to a visual extinction $A_V \sim 15$ -16 mag using the Bohlin et al. (1978) formula. We note, however, that the model of L1544 by Keto & Caselli (2010) and Keto et al. (2014) considers the extinction as a function of radius (within the core and not along the line-of-sight) and therefore the modelled A_V at this position is about half that measured along the line-of-sight ($A_V \sim 7.5$ -8 mag; see also Section 7).

From Table 2 and Figure 3 (lower panel), we find that CH_3O , CH_3OCH_3 , CH_3CHO are enhanced respectively by factors ~ 4 -5, ~ 2 and ~ 10 in the CH_3OH peak with respect to L1544's center (note that their associated 1σ uncertainties are lower than these enhancements). The other O-bearing COMs CH_3OCHO , $c\text{-}C_3H_2O$ and $HCCCHO$ show average abundances slightly higher toward the CH_3OH peak than toward the core center (by factors ~ 3), although they agree within the uncertainties. The same applies to the N-bearing COMs CH_2CHCN , CH_3NC and $HCCNC$, whose abundances lie within the uncertainties (Figure 3).

6 Upper limits to the abundance of pre-biotic COMs

The high-sensitivity spectra obtained toward L1544 allow us to provide stringent upper limits to the abundance of pre-biotic COMs such as glycine, NH_2CHO and CH_3NCO . As shown in Table 2, the derived upper limits to the column density of glycine are factors 40-120 lower than the best upper limits obtained toward the Galactic Center ($\sim 4 \times 10^{14} \text{ cm}^{-2}$; Jones et al. 2007). Our most stringent upper limit to the abundance of glycine in L1544 ($\sim 6 \times 10^{-11}$; Table 2) is also a factor of 5 lower than that inferred for the outer envelope of IRAS16293-2422 ($\sim 3 \times 10^{-10}$; Ceccarelli et al. 2000). Stacking analysis of the glycine lines with similar expected intensities in our frequency setup would reduce the rms noise level by a factor of ~ 3 (10 lines are covered), which implies an upper limit of $\sim 2 \times 10^{-11}$. This upper limit is close to the glycine abundance assumed by Jiménez-Serra et al. (2014) for the detectability of this molecule in pre-stellar cores ($\sim 3 \times 10^{-11}$). The upper limits derived for NH_2CHO [$(2.4\text{-}8.7) \times 10^{-13}$] and CH_3NCO [$(0.2\text{-}4.2) \times 10^{-11}$; Table 2] are consistent with

those measured in L1544 and B1-b by López-Sepulcre et al. (2015, 5×10^{-13}) and Cernicharo et al. (2016, 2×10^{-12}) respectively.

7 Chemical modelling of O-bearing COMs

In Section 5, we have reported abundance enhancements by factors ~ 2 -10 for CH_3O , CH_3OCH_3 and CH_3CHO as a function of distance in L1544. Other COMs such as CH_3OCHO may also be enhanced at larger radii although its derived abundances agree within the uncertainties (Section 5). In this Section, we model the chemistry of O-bearing COMs in L1544 by using the 1D physical structure derived by Keto & Caselli (2010) and Keto et al. (2014).

We use the chemical code of Vasyunin & Herbst (2013), which considers that COMs are formed via gas-phase ion-neutral and neutral-neutral reactions after the release of precursor molecules from dust grains via chemical reactive desorption. This code has been updated with a new multilayer treatment of ices, an advanced treatment of reactive desorption based on the experiments by Minissale et al. (2016), and new gas-phase reactions proposed by Shannon et al. (2013) and Balucani et al. (2015). The complete results from this modelling will be reported in Vasyunin et al., (in prep.).

The chemical evolution of COMs is followed over 3×10^6 years toward 129 points along the radius of the core to a distance ~ 65500 au. For all these positions, the density, temperature and A_V are taken from Keto et al. (2014). The initial molecular abundances are calculated by simulating the chemistry of a translucent cloud with density $n(\text{H})=10^2 \text{ cm}^{-3}$ and $T_{\text{gas}}=T_{\text{dust}}=20$ K over 10^6 years. The initial atomic abundances are the same as those of Vasyunin & Herbst (2013).

Our model shows that the abundances of COMs such as CH_3OCHO and CH_3OCH_3 change dramatically with time reaching maximum values at 10^5 - 3×10^5 years. The gas-phase COM radial profiles show their peak abundances at ~ 4000 au, *which roughly coincides with the position of the CH_3OH peak* (Bizzocchi et al. 2014). This is the location where CO starts freezing out onto dust grains in our model and it agrees well with the distance where CO depletion is observed in L1544 (see the drop in C^{17}O reported by Caselli et al. 1999). The CO depletion enhances the production of COM precursors on grain surfaces via hydrogenation reactions while, at the same time, the visual extinction is sufficiently high ($A_V \sim 7.5$ -8 mag; Section 5) to prevent the UV photo-dissociation of the chemically desorbed COM precursors by the external interstellar radiation field. UV photo-desorption is not efficient at this position in the core and, therefore, the release of COMs into the gas phase is dominated by chemical reactive desorption. Toward the center of the core, the abundances of COMs drop to undetectable levels ($\sim 10^{-14}$) as a result of the severe freeze out.

To compare the model results with our observations, one needs to sample all COM material along the line-of-sight toward the continuum and the CH_3OH peaks. *The amount of COM material sampled in the direction of the CH_3OH peak will be larger than toward the*

³Except NH_2CHO , none of the N-bearing COMs reported here are currently included in the chemical network of Vasyunin et al. (in prep.).

continuum peak. While toward the core's center COMs are found within a shell $R_{i-1} - R_i$ (with R the radius from the center and i the position in the grid with $i=1$ at the outermost shell), toward the CH_3OH peak COMs are sampled along a circle chord. For the core's center the COM column density, $N(\text{COM})$, is given by:

$$N(\text{COM}) = 2 \times \sum_{i=2}^n \left[\frac{n(H)_i \chi_i + n(H)_{i-1} \chi_{i-1}}{2} \right] \times (R_{i-1} - R_i) \quad (1)$$

with $n(H)_i$ the gas density at radial point i , χ_i the COM abundance, $(R_{i-1} - R_i)$ the shell width, and n the number of shells in the model ($n=129$). Toward the CH_3OH peak, $N(\text{COM})$ is calculated as:

$$N(\text{COM}) = 2 \times \sum_{i=2}^{n_{\text{peak}}} \left[\sqrt{R_{i-1}^2 - R_{\text{peak}}^2} - \sqrt{R_i^2 - R_{\text{peak}}^2} \right] \times \left[\frac{n(H)_i \chi_i + n(H)_{i-1} \chi_{i-1}}{2} \right] \quad (2)$$

where R_{peak} is the radial distance of the CH_3OH peak (4000 au), n_{peak} is the radial point closest to this peak, and R_i and R_{i-1} are the radii at positions i and $i-1$. $N(\text{COM})$ are averaged over the beam of the IRAM 30 m telescope ($\sim 26''$), and the COM abundances are finally calculated by dividing the average $N(\text{COM})$ by the $N(H_2)$ obtained following the same method ($4.0 \times 10^{22} \text{ cm}^{-2}$ for the continuum peak and $1.0 \times 10^{22} \text{ cm}^{-2}$ for the CH_3OH peak). Note that these values are similar to those used in Section 5. The best match with the observations is obtained at 10^5 years.

Table 2 and Figure 3 (upper panel) report the predicted abundances of CH_3O , CH_3OCHO , CH_3OCH_3 , CH_3CHO and NH_2CHO . The rest of O-bearing species (c- C_3H_2O , HCCCHO, CH_3NCO and glycine) are currently not included in the chemical network and their predictions are thus not reported. The modelled COM abundances reproduce the enhancements of CH_3OCH_3 and CH_3OCHO observed toward the CH_3OH peak within factors of 3 (Table 2 and Figure 3). For CH_3CHO , however, the model predicts a smaller enhancement than observed, although the modelled and observed CH_3CHO abundances agree within factors 2-3 for both positions. Large discrepancies are found for CH_3O and NH_2CHO (by factors ~ 5 -15 and ~ 100 -200, respectively; Table 2), which suggests that additional mechanisms are required to suppress the production of these COMs in our model.

In summary, we report new detections of COMs in L1544. Species such as CH_3O , CH_3CHO and CH_3OCH_3 are enhanced by factors ~ 2 -10 toward the CH_3OH peak with respect to the core's center. Other COMs such as CH_3OCHO may also be enhanced with increasing distance within the core (by factors ~ 3), although their abundance uncertainties are large. Despite the discrepancies found between the observed COM abundances and those predicted in our model, O-bearing COMs are predicted to present an abundance peak at 4000 au, which agrees well with the position of the CH_3OH peak and with the radial distance at which CO depletion is observed. All this shows that high-sensitivity observations of COMs

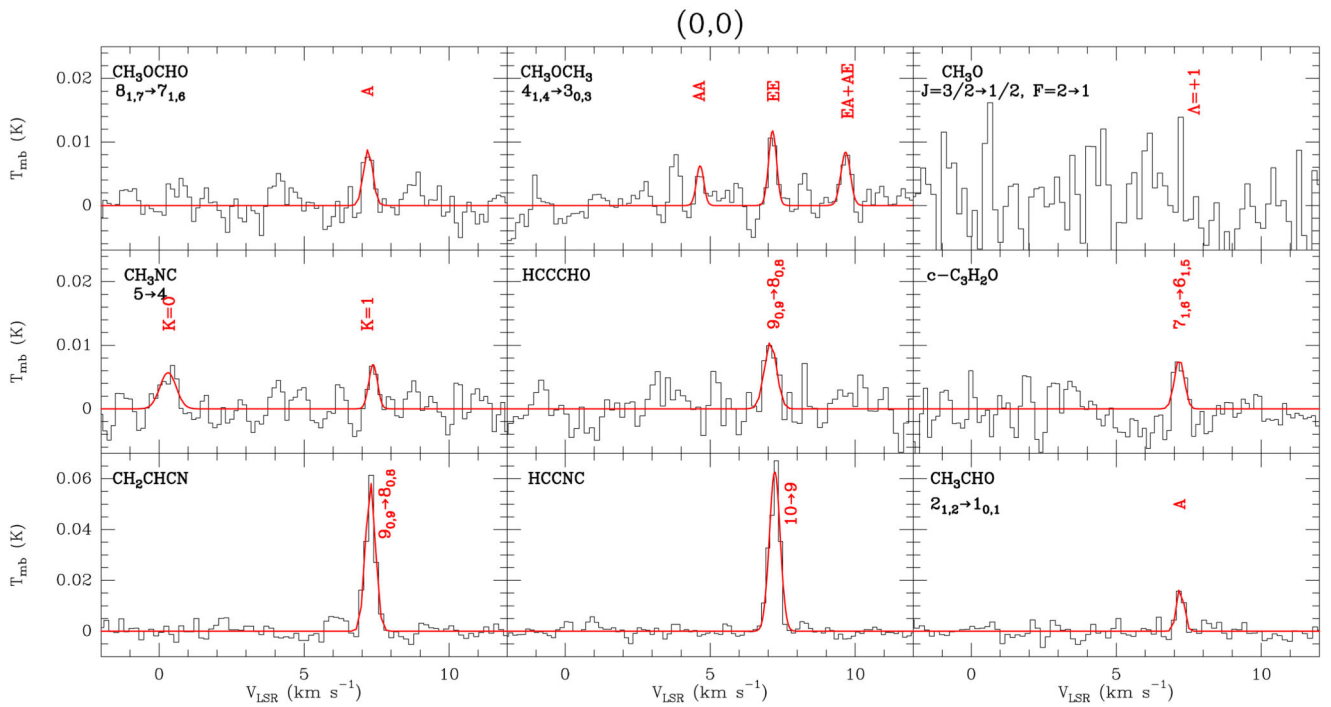
are strongly needed to put stringent constraints on chemical models and to step forward in our understanding of COM chemistry in the ISM.

Observations carried out under projects 129-14 and 001-16. IRAM is supported by INSU/CNRS (France), MPG (Germany) and IGN (Spain). We acknowledge the staff at the IRAM 30m telescope for the support provided during the observations. We also thank an anonymous referee for his/her careful reading of the manuscript and H. S. P. Müller for his help in the line identification. This research has received funding from the People Programme (Marie Curie Actions) of the EU's Seventh Framework Programme (FP7/2007-2013) under REA grant agreement PIFI-GA-2011-301538, and from the STFC through an Ernest Rutherford Fellowship (proposal ST/L004801/1). AV and PC acknowledge support from the European Research Council (ERC; Project PALs 320620). LT acknowledges partial support from the Italian Ministero dell'Istruzione, Università e Ricerca through the grant Progetti Premiali 2012 – iALMA (CUP C52I13000140001) and from Gothenburg Centre of Advanced Studies in Science and Technology through the program *Origins of habitable planets*.

References

- Bacmann A, Taquet V, Faure A, Kahane C, Ceccarelli C. *A&A*. 2012; 541:L12.
- Bacmann A, André P, Puget J-L, Abergel A, Bontemps S, Ward-Thompson D. *A&A*. 2000; 361:555.
- Balucani N, Ceccarelli C, Taquet V. *MNRAS*. 2015; 449:L16.
- Belloche A, Menten KM, Comito C, et al. *A&A*. 2008; 482:179.
- Belloche A, Garrod RT, Müller HSP, Menten KM. *Science*. 2014; 345:1584B. [PubMed: 25258074]
- Bizzocchi L, Caselli P, Spezzano S, Leonardo E. *A&A*. 2014; 569A:27B.
- Bohlin RC, Savage BD, Drake JF. *ApJ*. 1978; 224:132B.
- Bottinelli S, Ceccarelli C, Neri R, et al. *ApJ*. 2004; 615:354.
- Caselli P, Walmsley CM, Tafalla M, Dore L, Myers PC. *ApJ*. 1999; 523:L165.
- Caselli P, Keto E, Bergin EA, et al. *ApJ*. 2012; 759:L37.
- Ceccarelli C, Loinard L, Castets A, Tielens AGGM, Caux E. *A&A*. 2000; 357:L9C.
- Cernicharo J, Marcelino N, Roueff E, Gerin M, Jiménez-Escobar A, Muñoz Caro GM. *ApJ*. 2012; 759:L43.
- Cernicharo J, Kisiel Z, Tercero B, et al. *A&A*. 2016; 587:L4C.
- Charnley SB, Kress ME, Tielens AGGM, Millar TJ. *ApJ*. 1995; 448:232.
- Chuang K-J, Fedoseev G, Ioppolo S, van Dishoeck EF, Linnartz H. *MNRAS*. 2016; 455:1702.
- Crapsi A, Caselli P, Walmsley CM, Myers PC, Tafalla M, Lee CW, Bourke TL. *ApJ*. 2005; 619:379.
- Elias JH. *ApJ*. 1978; 224:857.
- Garrod RT, Weaver SLW, Herbst E. *ApJ*. 2008; 682:283.
- Herbst E, van Dishoeck EF. *ARA&A*. 2009; 47:427H.
- Hollis JM, Lovas FJ, Jewell PR. *ApJ*. 2000; 540:L107.
- Hollis JM, Remijan AJ, Jewell PR, Lovas FJ. *ApJ*. 2006; 642:933H.
- Ivlev AV, Röcker TB, Vasyunin A, Caselli P. *ApJ*. 2015; 805:59.
- Jiménez-Serra I, Testi L, Caselli P, Viti S. *ApJ*. 2014; 787:L33.
- Jones PA, Cunningham MR, Godfrey PD, Cragg DM. *MNRAS*. 2007; 374:579.
- Jørgensen JK, Favre C, Bisschop SE, Bourke TL, van Dishoeck EF, Schmalzl M. *APJL*. 2012; 757:L4.
- Keto E, Caselli P. *MNRAS*. 2010; 402:1625.
- Keto E, Rawlings J, Caselli P. *MNRAS*. 2014; 440:2616.
- Loison J-C, Agúndez M, Marcelino N, et al. *MNRAS*. 2016; 456:4101.

- López-Sepulcre A, Jaber AA, Mendoza E, et al. MNRAS. 2015; 449:2438.
- Marcelino N, Cernicharo J, Agúndez M, et al. ApJ. 2007; 665:L127.
- Maret S, Hily-Blant P, Pety J, Bardeau S, Reynier E. A&A. 2011; 526:47.
- Martín S, Krips M, Martín-Pintado J. A&A. 2011; 527A:36M.
- Minissale M, Moudens A, Baouche S, Chaabouni H, Dulieu F. MNRAS tmp.. 2016:155M.
- Müller HSP, Schlöder F, Stutzki J, Winnewisser G. J Mol Struct. 2005; 742:215.
- Öberg KI, Bottinelli S, Jorgensen JK, van Dishoeck EF. ApJ. 2010; 716:825O.
- Pickett HM, Poynter RL, Cohen EA, Delitsky ML, Pearson JC, Müller HSP. J Quant Spectrosc & Rad Transfer. 1998; 60:883.
- Rawlings JMC, Williams DA, Viti S, Cecchi-Pestellini C. MNRAS. 2013; 430:264.
- Reboussin L, Wakelam V, Guilloteau S, Hersant F. MNRAS. 2014; 440:3557.
- Remijan AJ, Markwick-Kemper A, ALMA Working Group on Spectral Line Frequencies. Bulletin of the American Astronomical Society. 2007; 39:963.
- Requena-Torres MA, Martín-Pintado J, Martín S, Morris MR. ApJ. 2008; 672:352.
- Rivilla VM, Fontani F, Beltrán MT, Vasyunin A, Caselli P, Martín-Pintado J, Cesaroni R. ApJ. 2016 [arXiv:1605.06109](https://arxiv.org/abs/1605.06109).
- Shannon RJ, Blitz MA, Goddard A, Heard DE. NatCh. 2013; 5:745.
- Spezzano S, Bizzocchi L, Caselli P, Harju J, Brünken S. A&A. 2016 accepted, [arXiv:1607.03242](https://arxiv.org/abs/1607.03242).
- Vastel C, Ceccarelli C, Lefloch B, Bachiller R. ApJ. 2014; 795:L2.
- Vasyunin AI, Herbst E. ApJ. 2013; 769:34.
- Ward-Thompson D, Motte F, Andre P. MNRAS. 1999; 305:143.

**Fig. 1.**

Sample of COM lines detected toward L1544's dust continuum peak. Red lines show the Gaussian line fits derived for the COM transitions (see Table 1). The CH_3O spectrum has been extracted from the ASAI data (Vastel et al. 2014).

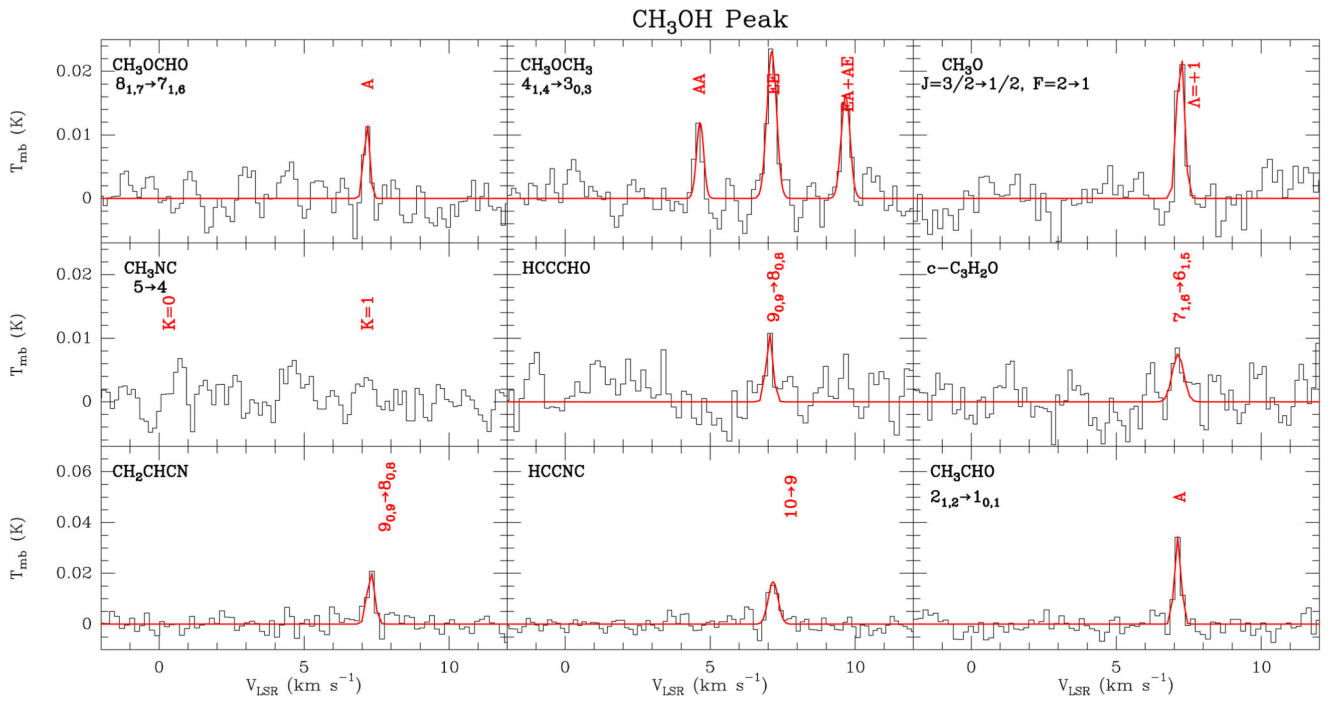


Fig. 2.
As in Figure 1, but for the position of the CH_3OH peak.

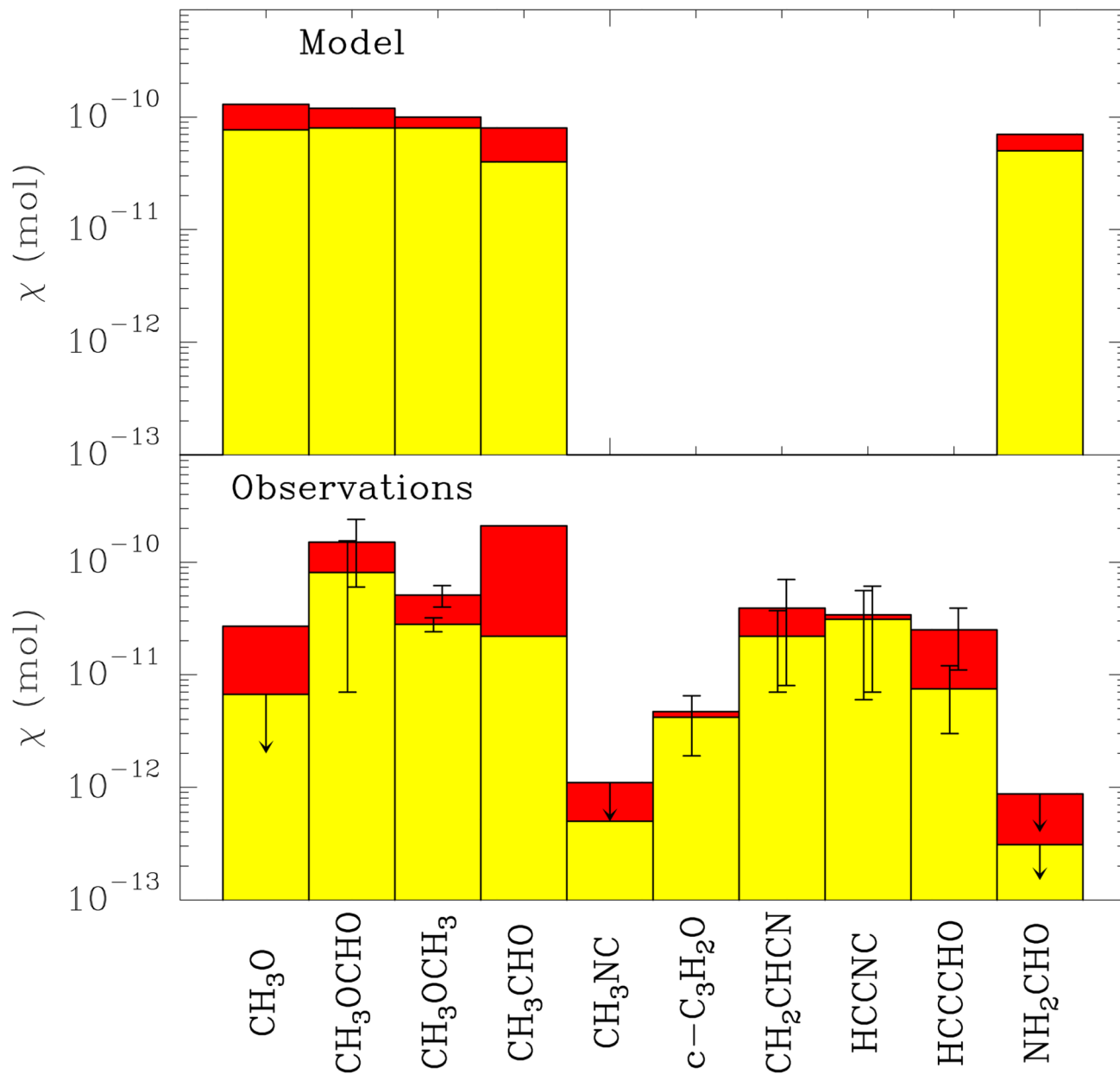


Fig. 3. Comparison of the observed and modelled abundance of COMs toward the continuum peak (in yellow) and the CH_3OH peak (in red; see Section 5). The abundances shown for c-C₃H₂O, HCCNC and HCCCHO are average values. Error bars correspond to 1σ uncertainties for CH₃OCHO, CH₃OCH₃ and CH₂CHCN, while they refer to the lower/upper abundance values estimated for c-C₃H₂O, HCCNC and HCCCHO (Table 2). Arrows indicate upper limit abundances.

Table 1
COM transitions covered in our observations and their derived line parameters

Species	Line	Frequency (MHz)	E_u (K)	g_u	A_{ul} (s^{-1})	$(0^{\circ}, 0^{\circ})$		CH_3OH peak				
						V_{LSR} ($km\ s^{-1}$)	ν ($km\ s^{-1}$)	T_{mb}^c (mK)	$Area^b$ ($mK\ km\ s^{-1}$)	V_{LSR} ($km\ s^{-1}$)	ν ($km\ s^{-1}$)	T_{mb}^c (mK)
CH_3O^d	$F=1 \rightarrow 0, \Lambda=-1$	82455.98	4.0	3	6.5×10^{-6}	16.2	$3.5(0.9)$	$7.06(0.03)$	$0.3(0.1)$	10.8(2.4)
	$F=2 \rightarrow 1, \Lambda=-1$	82458.25	4.0	5	9.8×10^{-6}	15.9	$9.2(1.1)$	$7.21(0.02)$	$0.40(0.05)$	21.8(3.0)
	$F=2 \rightarrow 1, \Lambda=+1$	82471.82	4.0	5	9.8×10^{-6}	17.1	$7.8(1.0)$	$7.22(0.02)$	$0.30(0.05)$	24.3(2.9)
	$F=1 \rightarrow 0, \Lambda=+1$	82524.18	4.0	3	6.5×10^{-6}	15.0	$2.6(0.9)$	$7.14(0.06)$	$0.27(0.08)$	8.9(3.0)
CH_3OCHO	$9_{1,9} \rightarrow 8_{1,8} E$	100078.608	25.0	38	1.4×10^{-5}	$7.23(0.10)$	$0.42(0.2)$	$4.1(2.0)$	1.7	8.1
	$9_{1,9} \rightarrow 8_{1,8} A$	100080.542	25.0	38	1.4×10^{-5}	$7.22(0.19)$	$0.44(0.15)$	$4.4(1.7)$	$3.3(0.8)$	$7.16(0.03)$	$0.30(0.09)$	$10.4(2.6)$
	$8_{3,5} \rightarrow 7_{3,4} E$	100294.604	27.4	34	1.3×10^{-5}	5.4	$3.5(0.9)$	$7.20(0.04)$	$0.34(0.10)$	$9.9(2.5)$
	$8_{3,5} \rightarrow 7_{3,4} A$	100308.179	27.4	34	1.3×10^{-5}	7.2	1.4	6.9
	$8_{1,7} \rightarrow 7_{1,6} E$	100482.241	22.8	34	1.4×10^{-5}	5.7	$6.5(0.9)$	$7.17(0.02)$	$0.31(0.06)$	$19.6(2.7)$
	$8_{1,7} \rightarrow 7_{1,6} A$	100490.682	22.8	34	1.4×10^{-5}	$7.21(0.04)$	$0.37(0.07)$	$8.9(2.2)$	$3.0(0.7)$	$7.16(0.03)$	$0.23(0.06)$	$12.3(2.6)$
	$9_{0,9} \rightarrow 8_{0,8} E$	100681.545	24.9	38	1.5×10^{-5}	$7.16(0.11)$	$0.4(0.2)$	$4.1(2.8)$	1.6	7.5
	$9_{0,9} \rightarrow 8_{0,8} A$	100683.368	24.9	38	1.5×10^{-5}	$7.12(0.07)$	$0.54(0.14)$	$7.2(2.7)$	$3.3(0.7)$	$7.11(0.03)$	$0.24(0.05)$	$13.1(2.6)$
	CH_3OCH_3	$4_{1,4} \rightarrow 3_{0,3} EA^d$	99324.357	10.2	36	2.2×10^{-5}	$7.11(0.05)$	$0.38(0.10)$	$8.4(2.4)$	$6.2(1.2)$	$7.11(0.03)$	$0.36(0.08)$
$4_{1,4} \rightarrow 3_{0,3} AE^d$		99324.359	10.2	54	3.3×10^{-5}
$4_{1,4} \rightarrow 3_{0,3} EE$		99325.208	10.2	144	8.9×10^{-5}	$7.15(0.03)$	$0.32(0.07)$	$11.55(2.2)$	$9.6(1.2)$	$7.12(0.02)$	$0.39(0.06)$	$23.5(3.1)$
$4_{1,4} \rightarrow 3_{0,3} AA$		99326.058	10.2	90	5.5×10^{-5}	$7.22(0.09)$	$0.3(0.2)$	$5.4(2.5)$	$3.7(1.1)$	$7.12(0.05)$	$0.29(0.09)$	$12.0(3.7)$
$6_{2,5} \rightarrow 6_{1,6} EA^d$		100460.412	24.7	52	1.8×10^{-5}	5.8	1.8	7.8
$6_{2,5} \rightarrow 6_{1,6} AE^d$		100460.437	24.7	78	2.6×10^{-5}
CH_3CHO	$6_{2,5} \rightarrow 6_{1,6} EE$	100463.066	24.7	208	7.0×10^{-5}	5.7	$1.4(0.8)$	$7.16(0.07)$	$0.26(0.16)$	$5.2(2.6)$
	$6_{2,5} \rightarrow 6_{1,6} AA$	100465.708	24.7	130	4.4×10^{-5}	6.3	1.8	7.8
	$2_{1,2} \rightarrow 1_{0,1} E$	85584.260	5.0	10	2.2×10^{-6}	$7.12(0.04)$	$0.32(0.10)$	$10.9(2.6)$	$12.8(1.1)$	$7.18(0.01)$	$0.31(0.04)$	$39.0(3.1)$
	$2_{1,2} \rightarrow 1_{0,1} A$	84219.764	5.0	10	2.4×10^{-6}	$7.21(0.02)$	$0.30(0.05)$	$17.4(2.5)$	$9.6(0.9)$	$7.12(0.01)$	$0.26(0.02)$	$34.4(3.0)$

Species	Line	Frequency (MHz)	E_u (K)	g_u	A_{ul} (s^{-1})	$(0^+, 0^+)$						CH ₃ OH peak		
						Area ^{a,b} (mK km s ⁻¹)	V_{LSR} (km s ⁻¹)	ν (km s ⁻¹)	T_{mb}^c (mK)	Area ^{a,b} (mK km s ⁻¹)	V_{LSR} (km s ⁻¹)	ν (km s ⁻¹)	T_{mb}^c (mK)	
	$2_{1,1} \rightarrow 1_{0,1} E$	87109.504	5.2	10	1.3×10^{-7}	1.4	6.5	1.7	7.7
	$2_{2,0} \rightarrow 3_{1,3} A$	87146.655	11.8	10	2.9×10^{-7}	1.3	6.2	1.5	6.6
	$2_{2,0} \rightarrow 3_{1,3} E$	87204.278	11.9	10	1.1×10^{-7}	1.6	5.9	1.7	7.4
	$6_{3,4} \rightarrow 7_{2,5} A$	99141.294	24.4	10	7.1×10^{-7}	1.4	6.7	1.8(0.8)	6.95(0.03)	0.2(0.2)	...	8.1(3.0)
	$6_{3,4} \rightarrow 7_{2,5} E$	99490.149	24.3	10	6.1×10^{-7}	1.4	6.7	2.9(0.9)	7.33(0.07)	0.4(0.1)	...	6.3(2.3)
CH ₃ CN	$5_0 \rightarrow 4_0$	100526.541	14.5	44	8.1×10^{-5}	4.0(1.0)	7.15(0.09)	0.66(0.18)	5.7(2.3)	1.8	7.5
	$5_1 \rightarrow 4_1$	100524.249	21.5	44	7.8×10^{-5}	2.6(0.7)	7.38(0.05)	0.35(0.11)	7.0(2.2)	1.8	7.5
	$5_2 \rightarrow 4_2$	100517.433	42.7	44	6.8×10^{-5}	1.7	6.9	1.8	7.5
c-C ₃ H ₂ O	$6_{1,6} \rightarrow 5_{1,5} e$	79483.520	14.6	39	5.1×10^{-5}	7.7(1.4)	7.09(0.03)	0.38(0.08)	...	18.8(3.0)
	$7_{1,6} \rightarrow 6_{1,5}$	103069.925	21.1	45	1.1×10^{-4}	3.3(0.9)	7.18(0.06)	0.39(0.09)	8.0(2.8)	3.7(1.7)	7.1(0.1)	0.5(0.3)	...	7.6(3.4)
CH ₂ CHCN	$9_{0,9} \rightarrow 8_{0,8}$	84946.000	20.4	57	4.9×10^{-5}	24.78(1.0)	7.290(0.007)	0.397(0.019)	58.7(2.3)	6.6(1.1)	7.300(0.02)	0.290(0.06)	...	21.1(3.1)
	$9_{1,8} \rightarrow 8_{1,7}$	87312.812	23.1	57	5.3×10^{-5}	13.2(0.9)	7.245(0.012)	0.35(0.03)	35.3(2.4)	5.1(1.1)	7.20(0.06)	0.46(0.09)	...	10.4(2.7)
	$11_{0,11} \rightarrow 10_{0,10}$	103575.395	29.9	69	9.0×10^{-5}	7.8(0.8)	7.30(0.02)	0.42(0.05)	17.3(2.3)	1.8	8.7
HCCNC	$10 \rightarrow 9 f$	99354.250	26.2	63	4.6×10^{-5}	29.2(1.0)	7.227(0.005)	0.438(0.013)	62.7(1.6)	7.1(1.0)	7.17(0.03)	0.40(0.05)	...	16.5(2.2)
HCCCHO	$9_{0,9} \rightarrow 8_{0,8}$	83775.842	20.1	19	1.8×10^{-5}	5.5(1.2)	7.08(0.06)	0.49(0.11)	10.6(2.8)	3.2(1.2)	7.04(0.06)	0.28(0.12)	...	10.8(3.5)
NH ₂ CHO	$4_{0,4} \rightarrow 3_{0,3} g$	84542.400	10.2	11	4.1×10^{-5}	1.8	8.4	2.3	9.6
	$4_{1,3} \rightarrow 3_{1,2} g$	87848.915	13.5	11	4.3×10^{-5}	1.3	6.0	1.8	7.2
CH ₃ NCO	$10_{1,10} \rightarrow 9_{1,9}$	87506.605	29.0	21	3.0×10^{-5}	1.1	5.1	1.2	5.7
	$12_{-1,12} \rightarrow 11_{-1,11}$	103023.61	39.4	25	4.9×10^{-5}	1.3	6.3	1.6	7.5
Glycine	$6_{5,2} \rightarrow 5_{4,1}$	103294.648	15.2	39	1.6×10^{-6}	1.7	8.0	2.1	9.9
Conf I.	$6_{5,1} \rightarrow 5_{4,2}$	103297.993	15.2	39	1.6×10^{-6}	1.7	8.0	2.1	9.9

^aHyperfine components of the N=1-0, K=0, J=3/2 → 1/2 transition of CH₃O.

η Upper limits calculated as $3\sigma \times \sqrt{\Delta\nu} \times \delta\nu$, with σ the rms noise level, ν the linewidth and $\delta\nu$ the velocity resolution of the spectrum.

ζ_p The rms noise level, σ , is given in parenthesis. Upper limits to the peak intensities refer to the 3σ noise level

ρ The AE and EA transitions overlap. We only show the gaussian fit for one of the lines. In the rotational diagram of this species, the individual areas of the AE and EA transitions are calculated by weighting the blended area by the degeneracy $g_U \times g_L$ of every transition.

τ_c Transition not observed toward the continuum peak.

f Hyperfine structure not resolved.

g Hyperfine transitions blended. Spectroscopic information provided only for the brightest hyperfine component F=5-4.

Table 2

Excitation temperatures, column densities, and measured and modelled abundances of COMs in L1544

Species	(0'',0'')				CH ₃ OH peak			
	T _{ex} (K)	N _{obs} (cm ⁻²)	χ _{obs} ^c	χ _{mod} ^d	T _{ex} (K)	N _{obs} (cm ⁻²)	χ _{obs} ^c	χ _{mod} ^d
CH ₃ O	5-10 ^b	(2.8-3.6)×10 ¹¹	(5.1-6.7)×10 ⁻¹²	7.7×10 ⁻¹¹	8.0 ^e	4.0×10 ¹¹	2.7×10 ⁻¹¹	1.3×10 ⁻¹⁰
CH ₃ OCHO	5.1±2.3 ^a	(4.4±4.0)×10 ^{12a}	(8.1±7.4)×10 ⁻¹¹	8.0×10 ⁻¹¹	7.9±3.6	(2.3±1.4)×10 ¹²	(1.5±0.9)×10 ⁻¹⁰	1.2×10 ⁻¹⁰
CH ₃ OCH ₃	5.7±3.1	(1.5±0.2)×10 ¹²	(2.8±0.4)×10 ⁻¹¹	8.0×10 ⁻¹¹	7.6±3.7	(7.7±1.6)×10 ¹¹	(5.1±1.1)×10 ⁻¹¹	1.0×10 ⁻¹⁰
CH ₃ CHO	5.0 ^e	1.2×10 ¹²	2.2×10 ⁻¹¹	4.0×10 ⁻¹¹	7.8 ^e	3.2×10 ¹²	2.1×10 ⁻¹⁰	8.0×10 ⁻¹¹
CH ₃ NC	22.9 ^e	2.7×10 ¹⁰	5.0×10 ⁻¹³	...	5-10 ^b	(0.7-1.6)×10 ¹⁰	(0.5-1.1)×10 ⁻¹²	...
c-C ₃ H ₂ O ^f	5-10 ^b	(1.0-3.5)×10 ¹¹	(1.9-6.5)×10 ⁻¹²	...	8.0 ^e	7.0×10 ¹⁰	4.7×10 ⁻¹²	...
CH ₂ CHCN	5.8±0.9	(1.2±0.8)×10 ¹²	(2.2±1.5)×10 ⁻¹¹	...	5.0±1.4	(5.8±4.7)×10 ¹¹	(3.9±3.1)×10 ⁻¹¹	...
HCCNC	5-10 ^b	(0.3-3.0)×10 ¹²	(0.6-5.6)×10 ⁻¹¹	...	5-10 ^b	(1.0-9.1)×10 ¹¹	(0.7-6.1)×10 ⁻¹¹	...
HCCCHO	5-10 ^b	(1.8-6.3)×10 ¹¹	(0.3-1.2)×10 ⁻¹¹	...	5-10 ^b	(1.6-5.8)×10 ¹¹	(1.1-3.9)×10 ⁻¹¹	...
NH ₂ CHO	5-10 ^b	(1.3-1.7)×10 ¹⁰	(2.4-3.1)×10 ⁻¹³	5.0×10 ⁻¹¹	5-10 ^b	(1.0-1.3)×10 ¹⁰	(6.7-8.7)×10 ⁻¹³	7.0×10 ⁻¹¹
CH ₃ NCO	5-10 ^b	(0.8-6.3)×10 ¹¹	(0.2-1.2)×10 ⁻¹¹	...	5-10 ^b	(0.9-6.3)×10 ¹¹	(0.6-4.2)×10 ⁻¹¹	...
Glycine	5-10 ^b	(3.3-5.8)×10 ¹²	(0.6-1.1)×10 ⁻¹⁰	...	5-10 ^b	(4.2-9.5)×10 ¹²	(2.8-6.3)×10 ⁻¹⁰	...

^aErrors correspond to 1σ uncertainties in MADCUBAIJ.^bT_{ex} range assumed to calculate the total column densities from a single COM transition using MADCUBAIJ.^cMolecular abundances calculated by using an H₂ column density of 5.4×10²² cm⁻² for the continuum peak (see Section 5 for details) and of 1.5×10²² cm⁻² for the position of the CH₃OH peak (Spezzano et al. 2016)^dAbundances predicted by the model of Vasyunin et al. (in prep).^eFitting solutions could only be obtained by fixing T_{ex} within MADCUBAIJ.^fT_{ex} and N_{obs} calculated using Weeds.